Fluorescent Single-Walled Carbon Nanotube Aerogels in Surfactant-free Environments

Juan G. Duque,[†,‡] Christopher E. Hamilton,[§] Gautam Gupta,[‡] Scott A. Crooker,[⊥] Jared. J. Crochet,[‡] Aditya Mohite,[†,‡] Han Htoon,[†,‡] Kimberly A. DeFriend Obrey,[§] Andrew M. Dattelbaum,[‡,*] and Stephen K. Doorn[‡,*]

[†]Physical Chemistry and Applied Spectroscopy Group, Chemistry Division, [‡]Center for Integrated Nanotechnologies, Materials Physics and Applications Division, [§]Polymers and Coatings Group, Materials Science and Technology Division, and [⊥]National High Magnetic Field Laboratory, Los Alamos National Laboratory, Los Alamos New Mexico 87545, United States

ABSTRACT A general challenge in generating functional materials from nanoscale components is integrating them into useful composites that retain or enhance their properties of interest. Development of single walled carbon nanotube (SWNT) materials for optoelectronics and sensing has been especially challenging in that SWNT optical and electronic properties are highly sensitive to environmental interactions, which can be particularly severe in composite matrices. Percolation of SWNTs into aqueous silica gels shows promise as an important route for exploiting their properties, but retention of the aqueous and surfactant environment still impacts and limits optical response, while also limiting the range of conditions in which these materials may be applied. Here, we present for the first time an innovative approach to obtain highly fluorescent solution-free SWNT-silica aerogels, which provides access to novel photophysical properties. Strongly blue-shifted spectral features, revelation of new diameter-dependent gas-phase adsorption phenomena, and significant increase (approximately three times that at room temperature) in photoluminescence intensities at cryogenic temperatures all indicate greatly reduced SWNT–matrix interactions consistent with the SWNTs experiencing a surfactant-free environment. The results demonstrate that this solid-state nanomaterial will play an important role in further revealing the true intrinsic SWNT chemical and photophysical behaviors and represent for the first time a promising new solution- and surfactant-free material for advancing SWNT applications in sensing, photonics, and optoelectronics.

KEYWORDS: single-walled carbon nanotube · fluorescence · surfactant-free · silica aerogel · nanocomposite · low-temperature

The strong correlation that exists between the observed photophysical properties of single-walled carbon nanotubes (SWNTs) and environmental factors[1−4] has driven interest in their potential for optical sensing, but also presents a challenge for advancing their use in optoelectronics and photonics applications.[5] Because the unique electronic and optical properties of SWNTs are highly sensitive to environmental effects, tuning interfacial behaviors between tubes and the local environment also presents a rich opportunity for engineering and optimizing their photophysical response. Further, reports have shown that small perturbations in the SWNT local environment have profound effects on SWNT emission due to disturbance of the exciton resonant energies.[2,3,6−8] Most often, the optical properties of SWNTs are investigated in aqueous surfactant suspensions,[9] yet the nature of these systems strongly perturb their observed properties. In particular, the presence of surfactant molecules or organic solvents changes the local dielectric environment, altering nanotube emission spectral line-widths and peak locations.[6−8,10−12] Surface structure and orientation of surfactants can further modulate the SWNT surface environment by defining surface access by other solution species. Such effects can be used to enhance PL quantum yields by creating a protective barrier to quenching species,[3,4] in some ways similar to surface passivation of nanocrystals. Despite the obvious benefits provided by aqueous surfactant suspensions of SWNTS, however, these perturbations present significant hurdles to evaluating intrinsic SWNT properties. Another drawback of aqueous suspensions is that the presence of water precludes the study of SWNT photoluminescence (PL) over any significant temperature range, especially at cryogenic temperatures. To overcome these limitations and investigate SWNT optical properties independent of environmental factors, researchers have employed noninteracting SWNT samples such as tubes suspended over trenches[1] or samples grown using a chemical vapor deposition-super-growth method.[13]

Percolation of SWNTs into aqueous gels such as silica,[14−17] agarose,[3,18] and hydrogels[19]

* Address correspondence to skdoorn@lanl.gov, amdattel@lanl.gov.

Received for review June 16, 2011 and accepted July 26, 2011.

Published online July 26, 2011
10.1021/nn202225k

is another important route for exploiting their unique properties. However, these systems provide only a limited understanding of the photophysical and electronic properties of SWNTs as the solvent molecules and the surrounding surfactant molecules needed to prepare SWNT-gels strongly perturb these properties. Supercritical drying of wet silica gels to form aerogels offers a potential alternative framework to obtain solution-free SWNT nanocomposites. Aerogels are important for a variety of applications due to their ultralow density, high porosity, and adjustable optical transparency.[20] SWNTs encapsulated in aerogels have previously been reported to enhance the mechanical strength, electrical conductivity, and Poisson ratio of the resulting composite material.[21,22] However, to date there are no reports of successfully prepared aerogels with SWNTs that maintain their photophysical properties upon supercritical drying. Such systems could yield the solution-free and surfactant-free environment needed to make fundamental optical measurements on ensembles of SWNTs, facilitating significant advance in the field of nanotube photophysics. Moreover, we anticipate that this system will be important in generating advanced materials for optoelectronics, nanophotonics, and photovoltaic applications.

Here, we introduce an approach to obtain highly fluorescent solution- and surfactant-free SWNT–silica aerogels and demonstrate that control over interfacial chemistry is essential to optimizing the PL response of the aerogel. The SWNT–aerogel photoluminescence features are blueshifted an average of 36 nm in emission and 20 nm in excitation from the initial dispersion, closely resembling the optical properties of noninteracting samples.[1,13] Moreover, we observe that the PL intensity substantially increases upon cooling from 300 to 3 K (in contrast to previous reports),[23–25] suggesting that the nanotubes are largely decoupled from the environment. In addition, when the SWNT–aerogels were exposed to gases, we observed a new diameter-dependent change in emission peak locations opposite to previous observations made in suspensions with varied dielectric environments. We present evidence that the magnitude of the aerogel peak shifts upon exposure to different gases and organic vapors is due to dissimilar diameter-dependent adsorption behavior. Each of these observations indicates that the SWNT network throughout the aerogel matrix experiences a local environment free of solvent and surfactant interactions.

RESULTS AND DISCUSSION

Aerogel Characteristics. Fluorescent SWNT-aerogels were prepared by first incorporating sodium deoxycholate (DOC) or sodium dodecylsulfate (SDS) suspended SWNTs into silica sol–gels as previously reported (see Methods).[15,17] Subsequent supercritical drying of the SWNT–sol gels was performed by replacing water in the gel with methanol and then removing the methanol in a supercritical carbon dioxide (CO_2) reactor, which yielded a monolithic low-density nanocomposite. After supercritical drying, the SWNT nanocomposites exhibit minimal shrinkage, good percolation of the SWNTs throughout the silica matrix, and optical transparency, as seen in Figure 1. Complete removal of solvent and the presence of silica were confirmed by Fourier transform infrared (FTIR) measurements (see Supporting Information, Figure S1). Typical aerogels displayed densities of 57 ± 2 mg/mL, surface areas of 1400 ± 100 m^2/g, and pore size distributions centered around 6 nm. Only minor differences in these properties are found in aerogels formed with and without SWNTs.

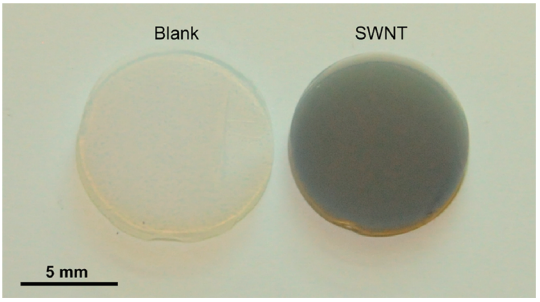

Figure 1. Optical image of aerogels. Aerogels without (blank) and with SWNTs.

The SWNT–aerogel composites are found to be of high optical quality. Absorbance spectra retain all of the expected exciton transitions with little scattering background from the matrix (see Supporting Information, Figure S2). Importantly, for all SWNT structural types (designated by the indices (*n,m*)) the composites retain many of the PL characteristics observed in the initial surfactant suspensions, as shown in the photoluminescence excitation (PLE) map in Figure 2a (and Supporting Information, Figure S2). A comparison of PL spectra (Figure 2b) from the aerogel (blue trace) and the initial suspension (red trace), shows that the PL signatures for all of the (*n,m*) semiconducting SWNTs present in the initial suspension are observed in the SWNT–aerogel. PL line widths in the aerogel are broader in comparison to the initial suspension (30 ± 3 and 22 ± 2 nm, respectively), indicating some degree of interaction with the matrix and possibly residual bundling due to the post-processing of the wet sol–gels to obtain the aerogels (see Supporting Information, section 3). Moreover, roughly 60% of the signal intensity from an initial DOC–SWNT suspension is retained in the aerogel material.

The aerogel matrices are also suitable for obtaining Raman spectroscopic data from the encapsulated SWNTs. Raman spectra (Figure 2c, 785 nm excitation) collected from aerogels made from SDS (black trace) and DOC (blue trace) suspensions display the typical bands expected for SWNTs,[26] with no accompanying interference near 400 cm^{-1}, where broad bands are typically observed in silica materials. Close inspection

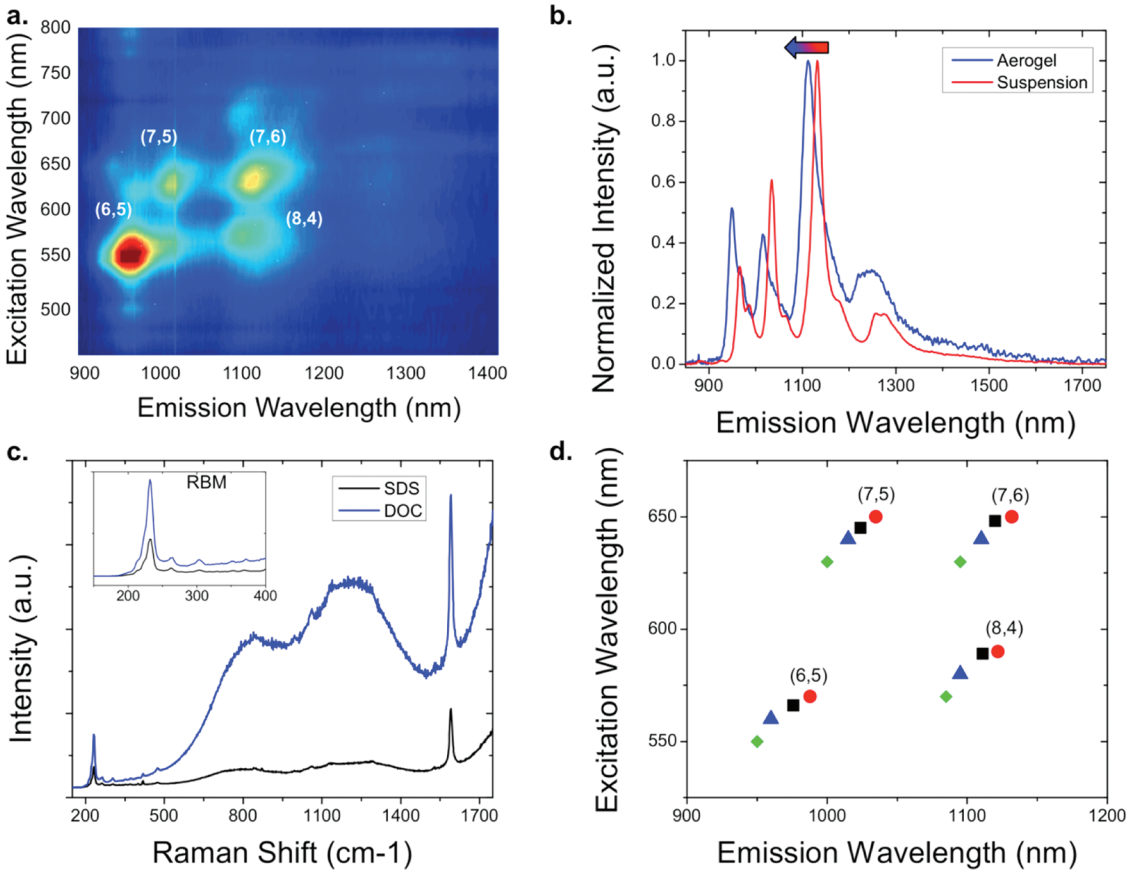

Figure 2. Spectroscopic characterization of SWNT–aerogel nanomaterials. (a) Photoluminescence excitation (PLE) map of a SWNT–aerogel (prepared from a DOC–SWNT suspension) with *(n,m)* structural indices of specific features identified. (b) Normalized PL spectra (658 nm excitation) of an initial DOC–SWNT suspension (red trace) and the resulting SWNT–aerogel (blue trace). (c) Raman spectra (785 nm excitation) of SWNT–aerogels made from SDS (black trace) and DOC (blue trace) SWNT suspensions. Broad peaks between 500 and ~1500 cm^{-1} originate from the fluorescence of small diameter semiconducting tubes, (5,4) at ~800 cm^{-1} and (6,4) at ~1250 cm^{-1}. (d) Comparison of emission and excitation peak locations for four different semiconducting SWNTs in DOC suspensions (red dots), in SDS suspensions (from ref 10, black square), in aerogels (blue triangle), and in calcined aerogels (green diamond).

of the radial breathing mode (RBM) region (between 100 and 400 cm^{-1}) shows minimal bundling of the SWNTs, as indicated by the weak response of the peak at 265 cm^{-1} at this excitation wavelength, relative to the peak at 237 cm^{-1}.[27] Minimization of bundling in the aerogel is critical to obtaining highly luminescent materials and may be adjusted by changing the level of SWNT loading. Decreasing the SWNT loading from ~10 ppm to ~3 ppm decreased the level of SWNT bundling and increased the PL intensity observed in the final aerogel by a factor of 2 (see Supporting Information Figure S3). Additionally, the appearance of the G-band at its typical location (~1591 cm^{-1}) and absence of a D-band (~1350 cm^{-1}) suggests minimal interaction between the silica matrix and SWNTs, as well as a low level of electronic doping and defects.[26] It is important to note that storage in a desiccator was necessary to retain the photophysical properties of the aerogels for long periods of time, as absorption of ambient moisture causes redshifts and a decrease in PL intensity of the SWNT–aerogel composite. This can be attributed to the hygroscopic nature of silica. In moisture-containing SWNT–aerogels, partial restoration (~50%) of the emission and blueshift is obtained by placing the aerogel in a vacuum furnace overnight at 100 °C.

Changing the surfactant used for the initial SWNT suspension can significantly alter the optical properties of the resulting aerogel matrix. Interestingly, while aerogels made from SDS suspensions share similar PL peak emission wavelengths as those found in DOC-based aerogels, they exhibit only a few percent (2–3%) of the PL intensity seen in the initial suspensions. This is in contrast to the strong PL intensity obtained from the DOC aerogels (see Figure 2c and Supporting Information, Figure S4). Raman spectra indicate that the loss of PL intensity in the SDS-based aerogel is not due to an increased level of SWNT bundling, since integrated 237 cm^{-1}/265 cm^{-1} peak ratios (9.2 ± 0.5 and 8.9 ± 0.8 for the DOC and SDS aerogels, respectively) are similar in both matrices and indicate minimal bundling has occurred. Instead, loss of PL intensity of the SDS-based structures is likely due to an increased interaction between the SWNTs and the silica matrix. SWNT PL is known to be very sensitive to changes in local environment.[3]

At the single nanotube level, single-point interactions with the environment can compromise PL over lengths of ~120 nm,[18] and thus have the potential to impact PL intensity over large regions of the SWNT surface.

Recently,[17] we proposed a model suggesting that the amphiphilic nature of DOC allows strong intermolecular hydrogen bonding between DOC molecules, resulting in the formation of a rigid and stable surfactant assembly that protects the SWNT surface. In contrast to DOC, the flexible linear hydrocarbon tail of SDS molecules results in a loosely packed surfactant structure that undergoes a greater degree of dynamical fluctuation, leading to greater interaction between the SWNTs and their immediate environment. Thus, during gelation the silica precursor molecules can penetrate the SDS assembly more readily than the DOC coating resulting in weaker PL intensities for the SDS-suspended tubes in contrast to DOC-wrapped tubes. The subsequent permanent loss of significant PL intensity on aerogel formation from SDS suspensions strongly suggests that these increased SiO_2 interactions are locked-in during the supercritical-CO_2 drying process. Thus, dynamic solution-phase surfactant behaviors can be directly translated into the final aerogel structures. This surfactant dependence highlights the importance of control over the interfacial chemistry in optimizing the PL response of the aerogel.

A particularly significant observation is that the emission and excitation peak wavelengths (E_{11} and E_{22} transition, respectively) of the semiconducting SWNTs are significantly blueshifted in the final aerogel in comparison to the initial suspension. The emission and excitation wavelengths observed in the aerogel matrix are compared to those in the initial suspension, as well as to values from the literature for SDS−SWNT suspensions[10] in Figure 2d and Table 1. In the DOC-based aerogel, average blueshifts are ~22 nm and ~10 nm for E_{11} and E_{22}, respectively. The larger wavelength sensitivity in E_{11} indicates it can act as a sensitive probe of the degree of matrix interactions experienced in the aerogel environment. While the SDS-based aerogel shows an apparent smaller blue shift ($E_{11} \approx 6$ nm) from its parent suspension than the DOC-based aerogel, this value is artificially low since the SDS-suspension is already significantly blue-shifted in comparison to DOC. In using E_{11} wavelengths as a measure to compare the final matrix interactions, it is therefore more instructive to directly compare final E_{11} emission wavelengths. Inspection of Table 1 shows, for all chiralities, that E_{11} for DOC-based aerogels appears at significantly shorter wavelengths than for SDS-based aerogels. This result indicates the DOC-based matrix imparts a reduced perturbation on SWNT optical properties and further supports our finding that SWNTs in the SDS-based aerogels experience greater interaction with the matrix.

Remarkably, Figure 2d shows that the emission and excitation are blueshifted in the DOC-based aerogel (blue triangle) to a greater extent than SDS suspensions[10] (black squares), which are known to be the most blue-shifted of all the aqueous suspensions[28] (see Table 1 for summary). In fact, the resulting E_{11} and E_{22} peak positions even approach those found in known noninteracting samples such as individual SWNTs suspended over trenches[1] or grown using a chemical vapor deposition (CVD) supergrowth method[13] in the absence of dispersing molecules like surfactants or polymers. This observation strongly suggests that not only are SWNT interactions with the aerogel matrix minimized, but also that the SWNTs are experiencing a surfactant-free environment. However, because the shift is less than that seen in samples free of interactions, a small level of residual matrix interaction likely remains.

To further establish the degree of surfactant removal from the SWNTs during the aerogel-preparation procedure, we obtained PL of DOC−aerogel samples after heating to 400 °C for 4 h (in vacuum) in order to burn off any traces of surfactant left in the aerogels. This calcination process is often used to remove surfactant from mesostructured materials to prepare mesoporous systems.[29] Calcination does not appear to induce any intensity changes to the SWNT PL spectra, nor did it cause any shrinkage of the aerogels. However, the peak location and excitation wavelengths after calcination were further blueshifted from the initial as-prepared aerogel by an average of ~15 and ~10 nm in emission and excitation wavelengths, respectively (green diamond, Figure 2d and Supporting Information, Figure S5). This second blueshift after calcination translates to an overall blueshift of roughly 36 nm in emission (E_{11}) and 20 nm in excitation (E_{22}) from the initial DOC aqueous dispersion. These final shifts more closely approach those observed in the examples of noninteracting samples, implying that any residual surfactant remaining after the initial aerogel formation process is removed after calcination and the resulting PL originates from surfactant-free SWNTs. We use the following empirical formula[7] to quantify the change in the dielectric environment starting from a surfactant-suspension (with a dielectric constant (ε_2) of 3.3)[30] to an aerogel:

$$\delta E_{abs}(\varepsilon_1\varepsilon_2) \approx 43(\varepsilon_1^{-1.6} - \varepsilon_2^{-1.6}) \text{ meV} \qquad (1)$$

With δE_{abs}= 43 meV (average E_{11} blueshift after calcination), we obtain a dielectric constant within the aerogel of 0.92, which confirms that the tubes in the aerogel matrix are "seeing" an air environment free of surfactants.

Gas-Phase Modulation of SWNT PL Response. The high porosity and surfactant-free nature of the aerogels, coupled with the sensitivity of SWNT PL response to changes in local environment, presents the opportunity for use of the SWNT-aerogel composites in gas-phase sensing. As a further demonstration of this potential, changes in the PL response for four different (*n*,*m*)

TABLE 1. Comparison of Emission (E_{11} Transition) and Excitation (E_{22} Transition) Shifts for Various (*n*,*m*) SWNTs in Suspension and Encapsulated in Silica Aerogels

	E_{11} (nm)						E_{22} (nm)						calcined DOC aerogel			
	suspensions		aerogels		$E_{11Sus} - E_{11Aero}$ (nm)		suspensions		aerogels		$E_{22Sus} - E_{22Aero}$ (nm)				$E_{Sus} - E_{Aero}$ (nm)	
(*n*,*m*)	SDS	DOC	SDS	DOC	SDS δ_{11}	DOC δ_{11}	SDS	DOC	SDS	DOC	SDS δ_{22}	DOC δ_{22}	E_{11} (nm)	E_{22} (nm)	δ_{11}	δ_{22}
(8,3)	952	967	949	940	3	27	665	670	660	660	5	10	932	650	35	20
(6,5)	976	988	968	960	8	28	566	570	560	560	6	10	950	550	38	20
(7,5)	1024	1035	1021	1015	3	20	645	650	640	640	5	10	1000	630	35	20
(8,4)	1111	1122	1101	1095	10	16	589	590	580	580	9	10	1085	570	37	20
(7,6)	1120	1132	1115	1110	5	22	648	650	640	640	8	10	1095	630	37	20

SWNTs were probed as the local environment was modulated. Aerogel samples were placed in an evacuated chamber that was then backfilled with a variety of gases and organic vapors, including air, carbon dioxide (CO_2), tetrahydrofuran (THF), and diethyl ether (see Methods section for more details). A shift in the PL peak position was observed after gas exposure (Figure 3a). The magnitude of the shift was quantified by comparison to the PL peak location exhibited by the SWNT aerogels in vacuum. Although the resulting shifts were small (between 3 and 12 nm, Figure 3b), their magnitudes are consistent with reports of surfactant-suspended SWNTs in the presence of organic solvents.[11,12] The magnitude of the peak shifts also correlates with gas-phase concentrations. As an example, a stronger response is observed for ether in comparison to THF, with ether having the higher vapor pressure.

These observations highlight the sensitivity of the SWNTs to minor changes in the local microenvironment with changes in the local dielectric constant and suggest that concentration-dependent measurements of other gas molecules may be accomplished. Such gas sensing applications will be dependent on the rapid response and cyclability of the aerogel system. We also observed that the PL shifts observed in the presence of gases are highly reproducible and reversible. As seen in Figure 3c, alternating exposure to ether and a vacuum atmosphere resulted in completely reversible and consistently reproducible peak shifts. Similar results were obtained with the other gases represented in Figure 3b (data not shown). The PL shifts occur less than 1 min after exposure to ether (within the duration of the PL integration time) and with recovery occurring roughly 2−3 min after removal of the gases. The lag time observed after terminating the gas exposure can be attributed to the high surface area of the aerogel and the time that it takes to fully evacuate the gas from the vessel. We also found that reproducible results are obtained from aerogels that have been aged for several weeks in a water-free environment (such as in a desiccator) and also in aerogels that have been repeatedly cycled through exposure to different gases. These observations demonstrate the high durability and reproducibility, as well as rapid response of the SWNT−aerogels.

Environmental modulation of exciton transition energies in the past has been attributed to changes in the local dielectric environment of the SWNTs, which is expected to result in a significant SWNT diameter dependence in the observed response.[2,11,12] As seen for the four chiralities highlighted in Figure 3b, we also observed a diameter-dependent response, but surprisingly, the dependence is the reverse of that previously found in the presence of organic solvents[11,12] and in other systems.[2] Here, the larger diameter SWNTs showed an increased response. This is evidence that the diameter dependence in our observations does not originate in the expected diameter dependence for dielectric environment effects on exciton transition energies. Instead, the result suggests that the magnitude of the shift in the peak location is due to the different SWNT diameters exhibiting dissimilar adsorption behavior. Moreover, although the dielectric constants of the molecules studied vary greatly (1−8) in the liquid phase, their values in the gas phase at room temperature are quite close (±0.005).[31] Thus, the PL shifts are found to be the direct result of changes in the microenvironment of the SWNTs, but are dominated by concentration and adsorption effects.

It is interesting to note that the observed wavelength shifts show a nearly linear dependence on diameter for a specific adsorbate species (Figure 3b), suggesting the magnitude of the response has a simple dependence on nanotube surface area. Paired with the readily reversible adsorption/desorption behavior demonstrated in Figure 3c, this result suggests that the gas species we study experience no specific interactions with the SWNT surface, and adsorption may be described by a basic Langmuir isotherm.[32] Although, SWNT ensembles have been previously used to detect adsorption of different gases,[32,33] this is the first report that uses the intrinsic optical properties of tube ensembles to detect gas adsorption. The breakdown in this linear dependence observed for the smallest diameter tube shown (the (8,3) in Figure 3b) may indicate some level of specific interactions do arise as a result of higher curvatures acting less like a continuous surface for physisorption. The adsorption behavior illustrated here further supports our claim that the SWNTs experience a surfactant-free environment within the

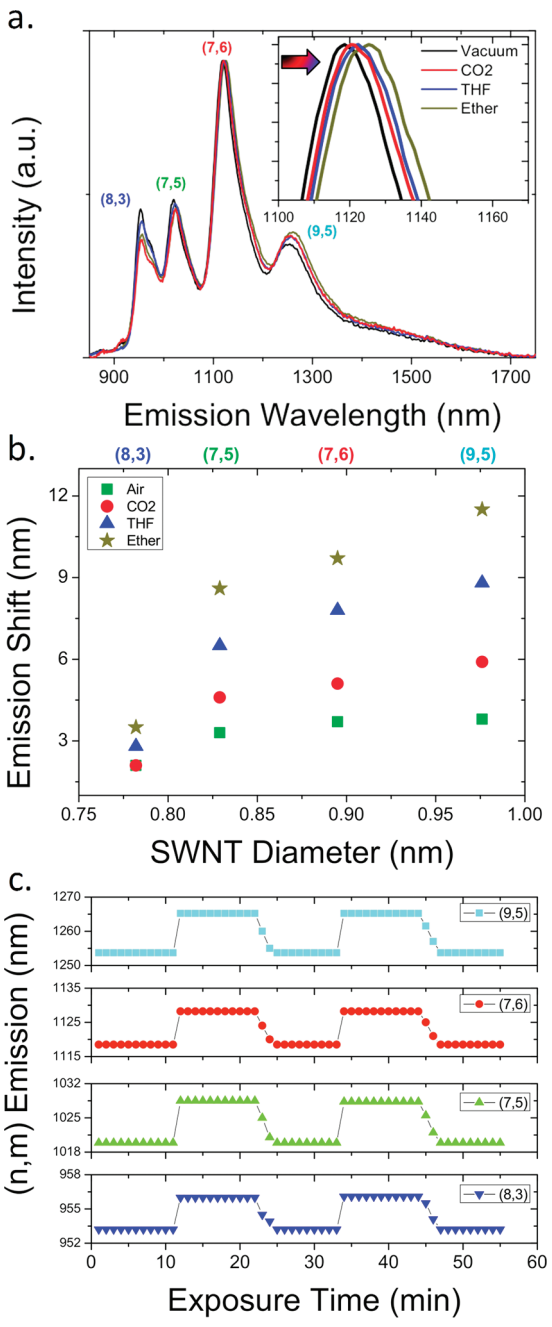

Figure 3. Gas-phase adsorption at the SWNT surface. (a) PL spectrum of aerogels in vacuum, and exposed to CO_2, THF, and ether vapors. (b) Shift in PL emission wavelength relative to the signal collected in vacuum as a function of SWNT diameter after exposure of SWNT-aerogels to air (green square), CO_2 (red dots), THF (blue triangle), and ether (yellow star). (c) Emission wavelength shifts for four different (*n*,*m*) SWNTs after alternating exposure to ether and vacuum: (9,5) light blue squares; (7,6) red dots; (7,5) green triangle; and (8,3) blue triangle.

aerogel matrix. Such simple adsorption behavior would be unlikely to result from a surfactant-coated system, in which adsorbate species must tunnel through a complex surface structure to gain access to the SWNT surface. It is important to note that we were able to observe this diameter-dependent adsorption behavior in our system since we have an ensemble of different (*n*,*m*) tubes in contrast to single tube examples, highlighting the broad range of applications of the SWNT–aerogel system.

Aerogel as Matrix for Fundamental Measurements. The observation of the novel diameter-dependent gas adsorption behavior highlights the importance the surfactant-free nature of the aerogel matrices will have in revealing new SWNT behaviors by enabling new fundamental optical measurements at the ensemble level. One important additional example is the ability to perform measurements at cryogenic temperatures. Such measurements in the absence of significant environmental perturbation have been limited at the ensemble level due to direct interaction of the SWNTs with previous matrix materials and the lack of suitable water-free matrices that exhibit high optical quality over extended temperature ranges. Our demonstration of the stability of the aerogel matrix to repeated pressure cycling and over broad temperature extremes (from nearly 700 to 3 K) illustrates their robustness for probing fundamental optical behaviors in a range of conditions. Here, we performed temperature-dependent PL measurements in a helium exchange gas cryostat from ~300 to ~3 K while resonantly exciting the (7,6) SWNT (see Methods for more details). As seen in Figure 4a, we observed a complex temperature dependent fluorescence intensity that was dominated by both the (8,4) and (7,6) tubes. However, by deconvoluting the spectra into the individual resonances we find two distinct behaviors. In Figure 4b we plot the relative spectral weight of the (8,4) and (7,6) fluorescence. The PL intensity of the (7,6) tube is found to increase monotonically as the temperature is decreased to approximately 30 K and then decreases slightly from 30 to 3 K. However, the intensity of the (8,4) tube is found to increase to a maximum at approximately 60 K and decreases to nearly 0 at 3 K. This is understood as a consequence of excitation being off resonance, where indirect absorption is strongly dependent on the availability of phonons.[34]

Qualitatively, the behavior of the (7,6) tube is similar to what has been previously reported for polymer-wrapped SWNTs on a substrate[25] or for SWNTs in a water/ice matrix[23] in which the PL intensity was also found to increase upon cooling to ~40 K followed by an intensity decrease with continued lowering of temperature to ~3 K. However, the degree of intensity decrease at the lowest temperatures is strikingly different. In the work of Matsunaga *et al.*[25] and Mortimer *et al.*,[23] they observed intensities at 4 K that are nearly the same as those found at room temperature. In our data, however, the intensity of the (7,6) tube at 4 K is approximately three times larger than what is found at room temperature. This difference can be understood as arising from a significantly slower relaxation of excitons from bright to dark states in our nanotubes, as a result of much weaker interaction with the aerogel environment than found in previous matrices. That is,

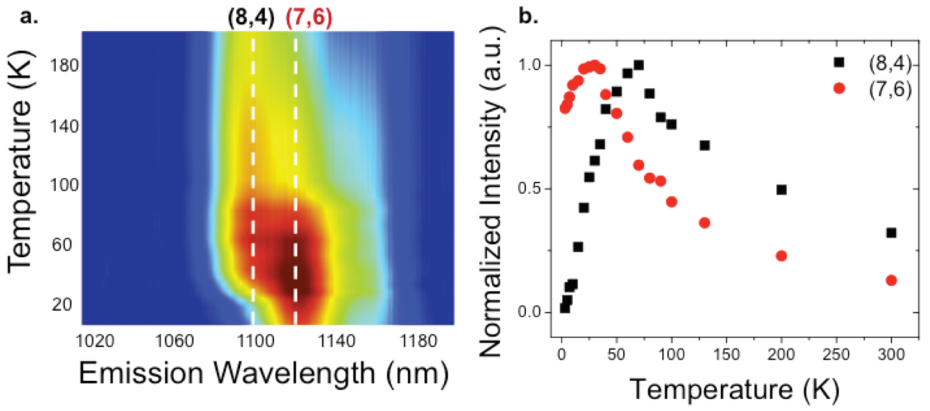

Figure 4. SWNT−aerogel PL intensity dependence on temperature. (a) Ensemble PL emission spectra of an aerogel as a function of temperature from ~200 to ~3 K excited at 658 nm and 30 s integration time. (b) Deconvoluted changes in PL intensity as a function of temperature from ~300 to ~3 K for the (8,4) and (7,6) tube.

the bright/dark exciton distribution is highly nonthermal, even at the lowest temperatures.

Recent experiments have shown that there exists a nonequilibrium (*i.e.,* nonthermal) distribution of bright and dark E_{11} excitons in nanotubes.[25,35] This is rationalized by the inability of phonons[36] or point defects[37] to efficiently generate relaxation or scattering pathways between bright and dark states. Overall, the radiative rate of bright excitons is expected to scale as $T^{(-1/2)}$, causing a gradual increase of PL intensity upon cooling from room temperature.[38] However, below temperatures of order the dark-bright exciton splitting (30−50 K), gradual freeze-out of excitons into dark states (and a commensurate quenching of the PL) is expected if, and only if, scattering between bright and dark states is efficient and the excitons remain in thermal equilibrium. These scattering pathways are thought to arise from environmental interactions. In our aerogel nanocomposites where environmental interactions are minimized, bright excitons *cannot* relax efficiently to the dark state, causing a highly nonequilibrium exciton distribution and a correspondingly large PL intensity, even at low temperatures (see Supporting Information, Figures S6−S7). Our data shows a PL intensity that is approximately three times larger at 4 K than at 300 K (in contrast to the much smaller ratio observed from nanotubes in polymers and ice matrices in previous work[23,25]), further supporting our conclusion that the SWNT-aerogel environment is surfactant-free, with significantly reduced matrix interactions. We are currently examining this behavior in more detail by investigating the temperature-dependent PL response in tailored SWNT−aerogels with different degrees of environmental perturbation.

In conclusion, we have developed a new and robust photoluminescent SWNT−aerogel matrix free of surfactants and solvent. The aerogels showed an overall blueshift in emission and excitation of roughly 35 and 20 nm after calcination in comparison to the initial dispersion, respectively. These blueshifts correspond to a dielectric environment approximately the same as that expected for air, further supporting the claim of a surfactant-free environment. The absence of surfactants at the tube surface enables the SWNT aerogel samples to undergo gas adsorption behavior with a strong diameter dependence. Moreover, we observed an approximately three times higher photoluminescent intensity at cryogenic temperatures in comparison to that at room temperature. These observations suggest that the SWNT−aerogel matrix exhibits minimal interaction with the local environment, highlighting the important link between SWNT interfacial chemistry and underlying photophysical behavior of SWNTs. This type of material may play an important role in revealing the underlying principles governing SWNT photophysical behavior previously masked by interactions with the local environment. Moreover, the strong PL obtainable from this nanomaterial, coupled with tunable interactions and optical density can potentially lead to an important role for these composites in generating new material functionality. We anticipate that multifunctional complex assemblies with other materials such as quantum dots, metallic nanoparticles, and organic acceptor/donor molecules for photovoltaic applications can be realized through the unique properties of our SWNT−aerogel composite.

METHODS

SWNT Preparation. HiPco SWNTs (Rice University) were individualized by dispersing them with standard suspension procedures as follows. A 10 mg portion of raw HiPco (batch 189.2) SWNTs were dispersed in 20 mL of D_2O using sodium dodecylsulfate (SDS) or sodium deoxycholate (DOC) at 1.0 wt % surfactant concentration. The suspension procedures were slightly modified from previous reports,[9] utilizing reduced

sonication times and powers to minimize SWNT cutting and the formation of side-wall defects so that highly luminescent SWNTs could be obtained. Homogenization was done at 19000 rpm (X520 CAT or PowerGen 700D shear mixer) for 2 h, followed by tip sonication at 20−25 W for 4 min in a cold water bath (Cole Parmer CPX 750). The sample was then ultracentrifuged at 29 000 rpm (~144000*g*) for 4 h in a Beckmann-Coulter TH-641 swing bucket rotor in a Sorvall WX Ultra 80 centrifuge. Contamination of the supernatant with nanotube bundles was minimized by collecting only the top 70% of the supernatant.

Aerogel Preparation. SWNT−silica gels were prepared using surfactant-suspended SWNTs in DOC or SDS by a chemical vapor-into-liquid sol−gel process described previously, or by direct addition of small aliquots of TMOS into the suspensions.[16,17] The wet gels were allowed to age for 48 h (essential for condensation of silica precursors) prior to supercritical drying.

Chemical Vapor-into-Liquid Sol−Gel Preparation. Two vessels, one containing a SWNT suspension (1.5 mL; 1% DOC or SDS) and the other TMOS (0.5 mL) were placed in a sealed container having a diameter of approximately 6.5 cm and a height of approximately 2.5 cm for 1−6 h at room temperature. During this time, TMOS (being volatile at room temperature) evaporates and diffuses into the aqueous suspension containing SWNTs. Further hydrolysis and condensation occurs over a period of time.[39] The SWNT suspension infused with the silica precursor was then transferred to a polyethylene vial (22 mm diameter) and sealed. Gelation occurred after approximately 12 h.

Liquid-Phase Sol−Gel Preparation. A SWNT suspension (2 mL; 1% DOC or SDS) and TMOS (200 μL) were combined and sealed in a vial. The mixture was shaken vigorously for 30 s and set aside. After 5 min, 1.5 mL was decanted from the top of the mixture (TMOS had settled to the bottom of the vial) and added to a polyethylene vial (22 mm diameter). The vial was sealed and gelation occurred within 10 min (total gel time approximately 15 min).

After aging the gels for at least 48 h, the vials containing the wet SWNT-silica gels were then filled with methanol (approximately 6 mL). The supernatant was discarded after 48 h and replaced with a second 6 mL aliquot of methanol (this process was repeated twice more to exchange water for methanol). Supercritical CO_2 drying of the SWNT-silica gels was then performed.

CO_2 Supercritical Drying. SWNT-silica gels infused with methanol were placed in a critical-point drier (Polaron, Quorum Technologies, Ltd., West Sussex, UK) and covered with methanol. The pressurized chamber was sealed and then filled with liquid carbon dioxide (10 °C, 51 atm). Over 24 h, methanol was periodically drained from the bottom of the vessel while maintaining pressure. After methanol had been completely exchanged by CO_2, the vessel was heated to 40 °C. During heating, the pressure was maintained at 90 atm by periodically releasing CO_2. After reaching 40 °C, the vessel was slowly depressurized (over 2−5 h) while maintaining temperature.

Density, Surface Area, and Porosity of Aerogel Matrices. Density was calculated gravimetrically. Nitrogen adsorption measurements were obtained at 77 K using a Quantachrome Autosorb surface area analyzer. Surface area was determined by Brunauer−Emmett−Teller (BET) multipoint analysis and pore size distribution by Barrett−Joyner−Halenda (BJH) theory.

Optical Characterization. Photoluminescence excitation (PLE) maps, fluorescence, and absorbance spectra were obtained from solutions, wet gels, and aerogels adjusted to roughly the same SWNT concentration (10 ppm). All optical spectra were normalized to concentration. Absorbance spectra were recorded on a Varian Cary 6000i instrument between 400 and 1400 nm at a rate of 2 nm per second. Emission spectra were obtained with excitation wavelengths between 450 and 800 nm using a xenon lamp coupled to a monochromator system with 10 nm bandpass and 5 nm excitation steps. The emission intensities were recorded between 900 and 1600 nm using a modified Nicolet NXR-9600 FT-IR spectrometer equipped with a liquid-N_2 cooled germanium detector. Spectra were obtained as averages of 100 scans, with a spectral resolution of 6 cm^{-1}. SWNT fluorescence spectra were also obtained with single line excitation using a 658 nm diode laser at 20 mW incident power. Raman measurements were performed using 10−15 mW of diode laser excitation at 785 nm. Spectra were obtained as 10 s integrations with a liquid-nitrogen-cooled charged couple device array coupled to a single grating monochromator. FT-IR spectra were collected using a Nicolet NXR-9600 FT-IR spectrometer. The FT-IR spectrometer was used in attenuated total reflectance (ATR) mode. Sample spectra were obtained as the sum of 100 scans, with subtraction of a 100-scan air background.

Gas Exposure Studies. Measurements of gas exposure effects on PL spectra were carried out in an airtight chamber (~2.5 cm^3) through which various gases and vapors from organic solvents were flowed. The emission spectra for the SWNT−aerogels under vacuum (~1×10^{-3} Torr) were first obtained, followed by exposure of the sample to either of the following conditions: air, CO_2, THF, or ether. A gas cylinder containing compressed air or CO_2 (~14 psig) was connected to one side of the sampling chamber and the gases were allowed to flow into the cell until the chamber was completely filled and reached the same pressure as the gas cylinder. Subsequently, PL measurements were performed. For the organic vapors (THF and ether), a 5 mL vial containing 2 mL of the respective organic solvent was attached to a 20 mL evacuated vial, which was then connected to one side of the evacuated sampling chamber (a slight negative pressure was imparted on the vial containing the organic solvent to minimize any trace of ambient air). The organic vapors were allowed to flow from the vial into the cell. The changes in PL peak location after addition of gases with respect to vacuum were obtained and plotted as a function of SWNT diameter.

Calcination. Calcination was performed inside a vacuum oven by increasing the temperature of the oven at a constant rate of 1 °C per minute up to 400 °C. The temperature was held constant at 400 °C for 4 h. The cooling rate was the same as the heating rate to prevent rapid cooling and degradation of the sample.

Cryogenic Measurements. PL spectroscopy from 3 to 300 K was performed in the variable-temperature insert (VTI) of a helium flow cryostat with direct optical access. Low power (~1 mW), defocused, continuous-wave light at 658 nm was used as the excitation source. The aerogel samples were mounted directly in the flowing helium vapor. Cernox thermometers on both the copper mounting block and on the VTI heat exchanger were used to ensure the SWNT temperatures (moreover, PL intensities at the lowest temperatures in helium vapor were unchanged when the samples were submerged in superfluid helium at ~2 K). Collected PL was dispersed in a 500 mm spectrometer and detected with a liquid nitrogen-cooled InGaAs linear array.

Acknowledgment. The authors thank the Smalley Institute for Nanoscale Science and Technology at Rice University for supplying SWNTs. This work was performed in part at the Center for Integrated Nanotechnologies, a U.S. Department of Energy, Office of Basic Energy Sciences user facility, and supported in part by LANL-LDRD funding. J.G.D. acknowledges support of the LANL-LDRD Director's Postdoctoral Fellowship. A.M.D. thanks the U.S. Department of Energy, Office of Basic Energy Sciences for partially supporting this work.

Supporting Information Available: FTIR, UV−vis−NIR absorbance, Raman, and fluorescence spectra of SWNT suspensions, wet gel and aerogel composites. In addition, detailed discussion of surfactant dependence, calcination effects, and temperature dependence of PL intensity. This material is available free of charge *via* the Internet at http://pubs.acs.org.

REFERENCES AND NOTES

1. Lefebvre, J.; Fraser, J. M.; Homma, Y.; Finnie, P. Photoluminescence from Single-Walled Carbon Nanotubes: A Comparison between Suspended and Micelle-Encapsulated Nanotubes. *Appl. Phys.* **2004**, *78*, 1107–1110.
2. Walsh, A. G.; Vamivakas, A. N.; Yin, Y.; Cronin, S B.; Unlü, M. S.; Goldberg, B. B.; Swan, A. K. Screening of Excitons in Single, Suspended Carbon Nanotubes. *Nano Lett.* **2007**, *7*, 1485–1488.
3. Duque, J. G.; Pasquali, M.; Cognet, L; Lounis, B. Environmental and Synthesis-Dependent Luminescence Properties of Individual Single-Walled Carbon Nanotubes. *ACS Nano* **2009**, *3*, 2153–2156.

4. Ju, S.-Y.; Kopcha, W. P.; Papadimitrakopoulos, F. Brightly Fluorescent Single-Walled Carbon Nanotubes *via* an Oxygen-Excluding Surfactant Organization. *Science* **2009**, *323*, 1319–1323.
5. Avouris, P.; Freitag, M.; Perebeinos, V. Carbon-Nanotube Photonics and Optoelectronics. *Nat. Photonics* **2008**, *2*, 341–350.
6. Ohno, Y.; Iwasaki, S.; Murakami, Y.; Kishimoto, S.; Maruyama, S.; Mizutani, T. Chirality-Dependent Environmental Effects in Photoluminescence of Single-Walled Carbon Nanotubes. *Phys. Rev. B* **2006**, *73*, 235427.
7. Ohno, Y.; Maruyama, S.; Mizutani, T. Environmental Effects on Photoluminescence of Single-Walled Carbon Nanotubes. *Carbon Nanotubes*; Marulanda, , J. M., Ed.; Intech: Croatia, **2010**.
8. Miyauchi, Y.; Saito, R.; Sato, K.; Ohno, Y.; Iwasaki, S.; Mizutani, T.; Jiang, J.; Maruyama, S. Dependence of Exciton Transition Energy of Single-Walled Carbon Nanotubes on Surrounding Dielectric Materials. *Chem. Phys. Lett.* **2007**, *442*, 394–399.
9. O'Connell, M. J.; Bachilo, S. M.; Huffman, C. B.; Moore, V. C.; Strano, M. S.; Haroz, E. H.; Rialon, K. L.; Boul, P. J.; Noon, W. H.; Kittrell, C.; *et al*. Band Gap Fluorescence from Individual Single-Walled Carbon Nanotubes. *Science* **2002**, *297*, 593–596.
10. Bachilo, S. M.; Strano, M. S.; Kittrell, C.; Hauge, R. H.; Smalley, R. E.; Weisman, R. B. Structure-Assigned Optical Spectra of Single-Walled Carbon Nanotubes. *Science* **2002**, *298*, 2361–2366.
11. Choi, J. H.; Strano, M. S. Solvatochromism in Single-Walled Carbon Nanotubes. *Appl. Phys. Lett.* **2007**, *90*, 223114.
12. Silvera-Batista, C. A.; Wang, R. K.; Weinberg, P.; Ziegler, K. J. Solvatochromic Shifts of Single-Walled Carbon Nanotubes in Nonpolar Microenvironments. *Phys. Chem. Chem. Phys.* **2010**, *12*, 6990–6998.
13. Araujo, P. T.; Maciel, I. O.; Pesce, P. B. C.; Pimenta, M. A.; Doorn, S. K.; Qian, H.; Hartschuh, A.; Steiner, M.; Grigorian, L.; Hata, K.; *et al*. Nature of the Constant Factor in the Relation Between Radial Breathing Mode Frequency and Tube Diameter for Single-Wall Carbon Nanotubes. *Phys. Rev. B* **2008**, *77*, 241403(R).
14. Whitsitt, E. A.; Barron, A. R. Silica Coated Single Walled Carbon Nanotubes. *Nano Lett.* **2003**, *3*, 775–778.
15. Satishkumar, B. C.; Doorn, S. K.; Baker, G. A.; Dattellbaum, A. M. Fluorescent Single-Walled Carbon Nanotube/Silica Composite Materials. *ACS Nano* **2008**, *2*, 2283–2290.
16. Zamora-Ledezma, C.; Anez, L.; Primera, J.; Silva, P.; Etienne-Calas, S.; Anglaret, E. Photoluminescent Single-Wall Carbon Nanotube−Silica Composite Gels. *Carbon* **2008**, *46*, 1253–1255.
17. Duque, J. G.; Gupta, G.; Cognet, L.; Lounis, B.; Doorn, S. K.; Dattelbaum, A. M. A New Route to Fluorescent SWNT/Silica Nanocomposites: Balancing Fluorescence Intensity and Environmental Sensitivity . *J. Phys Chem. C* **2011**, available online, DOI: 10.1021/jp2012107.
18. Cognet, L.; Tsyboulski, D. A.; Rocha, J.-D. R.; Doyle, C. D.; Tour, J. M.; Weisman, R. B. Stepwise Quenching of Exciton Fluorescence in Carbon Nanotubes by Single-Molecule Reactions. *Science* **2007**, *316*, 1465–1468.
19. Barone, P. W.; Yoon, H.; Ortiz-Garca, R.; Zhang, J.; Ahn, J.-H.; Kim, J.-H.; Strano, M. S. Modulation of Single-Walled Carbon Nanotube Photoluminescence by Hydrogel Swelling. *ACS Nano* **2009**, *3*, 3869–3877.
20. Fricke, J.; Tillotson, T. Aerogels: Production, Characterization, and Applications. *Thin Solid Films* **1997**, *297*, 212–223.
21. Bryning, M. B.; Milkie, D. E.; Islam, M. F.; Hough, L. A.; Kikkawa, J. M.; Yodh, A. G. Carbon Nanotube Aerogels. *Adv. Mater.* **2007**, *19*, 661–664.
22. Aliev, A. E.; Oh, J.; Kozlov, M. E.; Kuznetsov, A. A.; Fang, S.; Fonseca, A. F.; Ovalle, R.; Lima, M. D.; Haque, M. H.; Gartstein, Y. N.; *et al*. Giant-Stroke, Superelastic Carbon Nanotube Aerogel Muscles. *Science* **2009**, *323*, 1575–1578.
23. Mortimer, I. B.; Nicholas, R. J. Role of Bright and Dark Excitons in the Temperature-Dependent Photoluminescence of Carbon Nanotubes. *Phys. Rev. Lett.* **2007**, *98*, 027404.
24. Shaver, J.; Kono, J.; Portugall, O.; Krstić, V.; Rikken, G. L. J. A.; Miyauchi, Y.; Maruyama, S.; Perebeinos, V. Magnetic Brightening of Carbon Nanotube Photoluminescence through Symmetry Breaking. *Nano Lett.* **2007**, *7*, 1851–1855.
25. Matsunaga, R.; Miyauchi, Y.; Matsuda, K.; Kanemitsu, Y. Symmetry-Induced Nonequilibrium Distributions of Bright and Dark Exciton States in Single Carbon Nanotubes. *Phys. Rev. B* **2009**, *80*, 115436.
26. Dresselhaus, M. S.; Dresselhaus, G.; Saito, R.; Jorio, A. Raman Spectroscopy of Carbon Nanotubes. *Phys. Rep.-Rev. Sec. Phys. Lett.* **2005**, *409*, 47–99.
27. O'Connell, M. J.; Sivaram, S.; Doorn, S. K. Near-Infrared Resonance Raman Excitation Profile Studies of Single-Walled Carbon Nanotube Intertube Interactions: A Direct Comparison of Bundled and Individually Dispersed HiPco Nanotubes. *Phys. Rev. B* **2004**, *69*, 235415.
28. Moore, V. C.; Strano, M. S.; Haroz, E. H.; Hauge, R. H.; Smalley, R. E. Individually Suspended Single-Walled Carbon Nanotubes in Various Surfactants. *Nano Lett.* **2003**, *3*, 1379–1382.
29. Kresge, C. T.; Leonowicz, M. E.; Roth, W. J.; Vartuli, J. C.; Beck, J. S. Ordered Mesoporous Molecular-Sieves Synthesized by a Liquid-Crystal Template Mechanism. *Nature* **1992**, *359*, 710–712.
30. Avouris, P.; Chen, J.; Freitag, M.; Perebeinos, V.; Tsang, J. C. Carbon Nanotube Optoelectronics. *Phys. Stat. Sol. (B)* **2006**, *243*, 3197–3203.
31. Weast, R. C. ; Lide, D. R. *CRC Handbook of Chemistry and Physics*; CRS Press: Boca Raton, FL, 1986; Vol. 67.
32. Lee, C. Y.; Strano, M. S. Understanding the Dynamics of Signal Transduction for Adsorption of Gases and Vapors on Carbon Nanotube Sensors. *Langmuir* **2005**, *21*, 5192–5196.
33. Kong, J.; Franklin, N. R.; Zhou, C.; Chapline, M. G.; Peng, S.; Cho, K.; Dai, H. Nanotube Molecular Wires as Chemical Sensors. *Science* **2000**, *287*, 622–625.
34. Elliott, R. J. Intensity of Optical Absorption by Excitons. *Phys. Rev.* **1957**, *108*, 1384–1389.
35. Gokus, T.; Cognet, L.; Duque, J. G.; Pasquali, M.; Hartschuh, A.; Lounis, B. Mono- and Biexponential Luminescence Decays of Individual Single-Walled Carbon Nanotubes. *J. Phys. Chem. C* **2010**, *114*, 14025–14028.
36. Perebeinos, V.; Tersoff, J.; Avouris, P. Radiative Lifetime of Excitons in Carbon Nanotubes. *Nano Lett.* **2005**, *5*, 2495–2499.
37. Tomio, Y.; Suzuura, H. Impurity-Induced Valley Mixing of Excitons in Semiconducting Carbon Nanotubes. *Phys. E* **2010**, *42*, 783–786.
38. Spataru, C. D.; Ismail-Beigi, S.; Capaz, R. B.; Louie, S. G. Theory and *ab Initio* Calculation of Radiative Lifetime of Excitons in Semiconducting Carbon Nanotubes. *Phys. Rev. Lett.* **2005**, *95*, 247402.
39. Gupta, G.; Rathod, S. B.; Staggs, K. W.; Ista, L. K.; Oucherif, K. A.; Atanassov, P. B.; Tartis, M. S.; Montano, G. A.; Lopez, G. P. CVD for the Facile Synthesis of Hybrid Nanobiomaterials Integrating Functional Supramolecular Assemblies. *Langmuir* **2009**, *25*, 13322–13327.